# A Density Functional Theory Based Analysis of Photoinduced Electron Transfer in a Triazacryptand Based $K^+$ Sensor

Edward A. Briggs and Nicholas A. Besley*

*School of Chemistry, University of Nottingham, University Park, Nottingham, NG7 2RD, UK.*

E-mail: nick.besley@nottingham.ac.uk

*To whom correspondence should be addressed

**Abstract**

The electronic structure and photoinduced electron transfer processes in a $K^+$ fluorescent sensor that comprises a 4-amino-naphthalimide derived fluorophore with a triazacryptand ligand is investigated using density functional theory (DFT) and time-dependent density functional theory (TDDFT) in order to rationalise the function of the sensor. The absorption and emission energies of the intense electronic excitation localised on the fluorophore are accurately described using a ΔSCF Kohn-Sham DFT approach, which gives excitation energies closer to experiment than TDDFT. Analysis of the molecular orbital diagram arising from DFT calculations for the isolated molecule or with implicit solvent cannot account for the function of the sensor and it is necessary to consider the relative energies of the electronic states formed from the local excitation on the fluorophore and the lowest fluorophore→chelator charge transfer state. The inclusion of solvent in these calculations is critical since the strong interaction of the charge transfer state with the solvent lowers it energy below the local fluorophore excited state making a reductive photoinduced electron transfer possible in the absence of $K^+$, while no such process is possible when the sensor is bound to $K^+$. The rate of electron transfer is quantified using Marcus theory, which gives a rate of electron transfer of $k_{ET}$=5.98 x $10^6$ $s^{-1}$.

**Key Words**: photoinduced electron transfer, density functional theory, $K^+$ sensor

# Introduction

Ions play an important role in many biological processes. The potassium cation ($K^+$) is the most abundant intracellular ion and is involved in processes including muscle contractions, nerve transmission and kidney function.[1,2] Furthermore, $K^+$ deficiency can be a sign of poor health and an indicator of many conditions and diseases.[3–5] It is important to be able to determine the concentration of ions such as $K^+$ in cells, and fluorescence based sensors provide one approach to achieving this. Fluorescent based sensors typically comprise two key parts, a chelator and a fluorescent reporting moiety, where the chelator selectively "traps" the ion of interest resulting in a significant enhancement or quenching of the fluorescence of the fluorophore component of the probe.[6]

Several examples of fluorescent chemosensors for ions have been reported,[6–8] many of these are based upon the BODIPY (4-bora-3a,4a-diaza-s-indacene) chromophore.[6,9,10] Substituted BODIPY molecules are of considerable interest since the observed photophysical properties are highly sensitive to the nature of the substitution, and there have been several recent computational studies concerned with the calculation of the absorption and emission properties of BODIPY based systems.[11–16] These include the incorporation of solvent via a polarised continuum model.[12,15] In this work we focus on a triazacryptand-based fluorescent sensor with a 4-amino-naphthalimide fluorophore reported by Zhou et. al.,[17] shown in Figure 1. This fluorescent probe is weakly fluorescent, but in the presence of $K^+$ it becomes strongly fluorescent. There are many photophysical processes that can lead to the quenching or enhancement of fluorescence. In **1** the change in fluorescence has been attributed to a reductive photoinduced electron transfer (PET) mechanism.[17] This process can be described as[6]

$$ {}^1A^* + D \rightarrow {}^1A^{\bullet -} + D^{\bullet +} \tag{1} $$

where ${}^1A^*$ represents the electronically excited 4-amino-naphthalimide fluorophore and D represents the electron donating triazacryptand system, and is illustrated schematically in Figure 2.

In the absence of $K^+$, the PET process occurs resulting in fluorescent quenching and the system returning to its ground state via a nonluminescent process. However, in the presence of $K^+$ the chelator is no longer able to donate electrons to the chromophore and the PET process does not occur resulting in a strong fluorescence. Oxidative PET is a related process and corresponds to

$$^1D^* + A \rightarrow {}^1D^{\bullet +} + A^{\bullet -} \tag{2}$$

where the excited electron of the fluorophore can be transferred to a low lying unoccupied orbital of the chelator.

The design and development of chemical sensors is challenging partly due to the complexity of the underlying photophysical processes. Quantum chemical calculations have a potentially valuable role to play in this area since they can provide a detailed picture of the electronic structure of the fluorescent probe molecules, giving insight into the relevant photophysical processes. The large size of the molecules involved precludes the use of accurate wave function based excited state methods such as multireference configuration interaction[18] and multiconfigurational perturbation theory[19] and density functional theory based approaches represent the most accurate alternative. A number of groups have studied the PET in fluorescent probes using Kohn-Sham density functional theory (DFT) and time dependent density functional theory (TDDFT).[10,20–23] The most common approach is to construct a molecular orbital diagram for the frontier molecular orbitals based upon the Kohn-Sham orbitals and their associated energies to determine whether PET and the associated fluorescence quenching or enhancement should occur.[20–22] This can often provide a picture that is consistent with the experimental observations, and can be used to rationalise the observed fluorescent properties of a chemical sensor.

In an analysis of this type, the difference in orbital energies is implicitly being used as a measure of the relative energies of the excited states associated with the various stages of the PET

process. Orbital energy differences often provide a poor measure of the energies of the respective excited states, and to determine these reliably it is necessary to use a genuine excited state electronic structure method, such as TDDFT. Recent work has used TDDFT calculations to analyse the fluorescence quenching by Hg(II) ion chelation and fluorescence enhancement by Zn(II) ion chelation in a PET sensor.[23] However, the application of TDDFT to study these systems is not without its pitfalls since many of the states involved will be charge transfer (CT) in nature, which represents a case where TDDFT with standard generalized gradient approximation (GGA) or hybrid exchange-correlation functionals are known to fail.[24] In this Paper, we investigate the PET in the $K^+$ sensor **1** using DFT, TDDFT and excited state Kohn-Sham DFT (eDFT). It is shown that different approaches can lead to different conclusions, with in some cases the correct behaviour predicted for the wrong reason. We find that to account for the PET in **1** correctly, it is necessary to use an appropriate excited state electronic structure method and include the influence of solvent.

# Computational Methods

The structure of **1** in its ground state was optimised with and without the $K^+$ ion using DFT with the B97-1 exchange correlation functional[25] and the 6-31G* basis set.[26,27] Figure 1 shows the molecular structure of the sensor used in the calculations. In experiment the sensor has an extended chain attached to the nitrogen atom of the fluorophore that is not well defined. This part of the structure plays no role in the function of the sensor and the chain is replaced by a single hydrogen atom. Excited state energies have been determined using TDDFT with the B97-1 and CAM-B3LYP[28] functionals. Excited singlet state energies can also be determined in a ΔSCF (or ΔKohn-Sham) approach using Kohn-Sham DFT where some additional constraint is imposed to prevent the variational collapse to the ground state. In this work we use a procedure known as the maximum overlap method (MOM),[29] which has been used successfully to model the excited states of a range of systems,[30–32] including BODIPY.[14] One issue with this approach is that open-shell singlet states are not described well by a single determinant leading to a significant underestimation

of the energy of some singlet excited states.[29] However, the spin-purification procedure wherein the energy of the excited state is given by[33]

$$E = 2E_S - E_T \tag{3}$$

where $E_S$ is the single determinant excited singlet state energy (as given by MOM) and $E_T$ is the energy of the corresponding triplet excited state can provide a good correction.[34] The structure of the excited states were also optimised using the MOM approach. Solvent was modelled using a polarisable continuum model (PCM) with parameters corresponding to water. All calculations were performed using the Q-Chem software package.[35]

# Results and Discussion

*Computed Transition Energies*

Figures 3 and 4 show the lowest unoccupied and highest occupied orbitals as given by a B97-1/6-31G* calculation for **1** with and without the $K^+$ ion. Without $K^+$ the lowest unoccupied molecular orbital (LUMO) is a $\pi^*$ orbital located on the fluorophore part of the molecule. The three highest occupied molecular orbitals (HOMOs) are localised on the chelator and the highest occupied orbital associated with the fluorophore is the HOMO-3 orbital which can be described as a $\pi$ orbital. The intense band observed in the absorption spectrum is localised on the fluorophore and arises from the HOMO-3→LUMO transition. With the inclusion of $K^+$, the intense transition localised on the fluorophore corresponds to excitation from the HOMO→LUMO+1. The LUMO is localised on the potassium ion and the other high lying occupied orbitals are localised on the fluorophore or the linking group between the fluorophore and chelating moiety.

Table 1 shows the computed transition energies of the intense fluorophore transition using various DFT based approximations. The calculated gas-phase transition energies are higher than the

experimental value of 2.76 eV.[17] Taking the difference in the relevant orbital energies ($\Delta\varepsilon$) gives a value of 3.76 eV. This is improved by TDDFT which gives values of 3.36 eV for the B97-1 functional. The long-range corrected functional CAM-B3LYP predicts transition energies that are about 0.4 eV higher in energy than for the standard hybrid functional, and close to the $\Delta\varepsilon$ value. In the ΔSCF calculations the initial orbitals were generated from the ground state orbitals where a $\beta$ electron is moved from the HOMO-3 orbital to the LUMO. Results are given for the spin-mixed determinant, denoted $\Delta SCF^{SM}$, and if post-SCF spin-purification has been applied, denoted $\Delta SCF^{SP}$. Both of these approaches give a lower transition energy that are closer to experiment. The spin-mixed approach gives 2.82 eV, however this is artificially too low and spin-purification gives a value of 3.20 eV which is consistent with TDDFT. Table 2 shows the variation of the computed absorption energy with improving the quality of the basis set for the sensor with no $K^+$ bound. These results indicate that changing from a double to triple zeta type basis set leads to changes in the computed excitation energies of up to 0.05 eV. The addition of diffuse basis functions gives a greater variation with changes in the computed excitation energies of up to 0.1 eV. Consequently, the transition energies predicted with 6-31G* should be converged with respect to the basis set quality to the order of about 0.1 eV.

The experimental value is measured in solution and the presence of solvent can influence the position of the absorption band. The dipole moment for the ground state ($\mu_{gs}$) is 7.58 D as given by DFT with the B97-1 functional and this increases to 9.01 D in the excited state arising from the fluorophore excitation. Consequently, a shift to lower energy would be expected in a polar solvent and using an implicit solvent model for water shows a shift to lower energy of about 0.1 eV. Our best calculation, $\Delta SCF^{SP}$(sol)-B97-1, predicts a value of 3.02 eV which lies within 0.3 eV of the experimental value. Once the sensor is complexed with $K^+$ there is only a modest effect on the fluorescent part of the molecule and only a little change in the excitation energy of the fluorophore. The different methods consistently predict a small increase of about 0.1 eV when $K^+$ is present. Optimization of the excited state structure allows the emission energy to be calculated. The cal-

culations give values of 2.48 eV and 2.24 eV for the $\Delta SCF^{SM}$-B97-1 and $\Delta SCF^{SM}$(sol)-B97-1 methods, respectively, which compare well with the experimental value of 2.41 eV.

*Analysis of PET Based Upon the Molecular Orbital Diagram*

Figure 5 shows a schematic orbital energy diagram based upon the Kohn-Sham orbital energies for the B97-1/6-31G* calculation for the ground electronic state where the orbitals have been partitioned according to whether they are localised on the fluorophore or the chelator and the orbital occupancies depicted correspond to after the excitation of the fluorophore. When no $K^+$ is present there are three occupied chelator orbitals that can facilitate electron transfer to the fluorophore which is consistent with a reductive PET process occurring. In contrast when $K^+$ is bound to the chelating part of the sensor, there are no occupied orbitals associated with the chelator present between the HOMO and LUMO of the fluorophore suggesting that a reductive PET process will not occur. This is consistent with an enhancement of the fluorescence of the sensor. However, there is an unoccupied chelator orbital that lies just below the LUMO of the fluorophore which opens up the possibility of an oxidative PET process occurring. Consequently, an analysis based upon the molecular orbitals would predict a reductive PET process in the absence of $K^+$ and an oxidative PET process in the presence of $K^+$. This would result in the sensor not fluorescing whether $K^+$ was present or not, which is not consistent with experiment. Consideration of the molecular orbitals from the CAM-B3LYP calculation leads to a similar conclusion. Also shown in Figure 5 are the molecular orbitals from the calculations with implicit solvent. For the sensor without $K^+$ the molecular orbital diagram is qualitatively similar to the gas-phase. For the case where $K^+$ is present occupied orbitals associated with the chelating part of the molecule are present between the HOMO and LUMO of the fluorophore and reductive PET remains a possibility.

*Analysis of PET Based Upon Excited State Calculations*

Based upon the above analysis we conclude that a simple consideration of the molecular orbitals and their energies is not sufficient to reliably predict whether a PET process will occur and it is necessary to consider the relative energies of the initial and final electronic states. For a PET process to occur, the energy of the resulting electronic state formed should be lower than the energy of the excited state formed by excitation of the fluorophore. For the $K^+$ sensor considered here, the final state corresponds to a CT state where the electron from the HOMO of the fluorophore has been excited to a virtual orbital associated with the chelating part of the molecule. Table 3 shows the computed transition energies for the lowest CT transition. We first consider the TDDFT results with the hybrid B97-1 functional. Without $K^+$ the transition energy for the lowest CT transition is 0.58 eV lower than for the local fluorophore transition, while with $K^+$ the lowest CT transition is higher in energy than the fluorophore transition. These results are consistent with the experimental observations that $K^+$ will lead to enhanced fluorescence. However, it is known that TDDFT with hybrid functionals can severely underestimate the energy of CT states. A $\Lambda$ analysis[24] gives a value of 0.00 for the CT transition compared to 0.68 for the local fluorophore transition, suggesting that the computed CT energy is unreliable. The long-range corrected functional CAM-B3LYP should provide a more accurate transition energy for the CT state, and gives a value of 4.36 eV. Consequently, with the CAM-B3LYP functional there is no CT state lower in energy than the state formed from the local excitation ($\Delta$E=3.76 eV) on the fluorophore suggesting that no PET process will occur. We note that this energy difference is considerably larger than 0.1 eV, which the approximate error associated with the basis set. Within a $\Delta$SCF methodology CT states can be described with a hybrid functional and it is not necessary to use a long-range corrected functional. A transition energy of 5.05 eV was obtained which is much higher than the local fluorophore transition and consistent with TDDFT with CAM-B3LYP. For the CT state, spin-purification has a very small effect on the transition energy since the triplet state has a similar energy to the singlet state and only the spin mixed transition energies are given. We note that converging the SCF process for the CT

state using the MOM procedure was problematic for **1** in the gas phase where variational collapse to the ground state could not be prevented using initial guesses based upon the ground state orbitals of the gas phase molecule. These problems were not experienced for the PCM solvent calculations and the gas phase value was obtained by using the converged orbitals for the CT state with the PCM as a starting point for the gas phase calculation. The dipole moment for the CT state is computed to be $\mu_{CT}$=82.3 D which is much higher than the 9.01 D for the excited fluorophore state. This suggests that there will be a greater interaction with a polar solvent for the CT state, raising the possibility that the relative ordering of the local fluorophore excitation and the lowest CT excitation may be changed by the solvent. The results for the ΔSCF calculation with the implicit solvent model predicts that this is the case and the energy of the CT state lies (ΔE=2.57 eV) below the local fluorophore excitation (ΔE=3.02 eV) . With $K^+$ present the lowest CT transition is higher in energy than the excited fluorophore state for all of the calculations including ΔSCF with solvent.

These calculations demonstrate that to reliably predict whether a PET process will occur in a metal ion sensor such as **1** it is necessary to use an appropriate excited state method that can accurately describe charge transfer states and also account for solvent at least at the level of an implicit solvent model. This can be achieved with DFT based ΔSCF approaches but could also be achieved with TDDFT with long-range corrected functionals. However, it is necessary to account for the solvent contribution to the exchange-correlation response and it is not sufficient to simply use solvent polarised orbitals in the TDDFT equations. There are other effects that remain neglected in these calculations. The sensor has a significant amount of conformational flexibility which is not captured by considering just a single structure. For smaller systems such as BODIPY it is possible to compute absorption and emission spectra through averaging over molecular structures generated in an ab initio molecular dynamics simulation.[14] However, such molecular dynamics calculations for a system as large as the $K^+$ sensor are prohibitively expensive and here we focus on establishing a computationally efficient approach to reliably predicting the PET processes. Similarly, more complex solvent models could be used, including using explicit solvent molecules[36] or more

elaborate continuum solvent models. The solvent shifts arising in the sensor are electrostatic in origin and arise from the very different dipole moments between the local fluorophore and charge transfer excitations and should be adequately described by the PCM solvent model used here.

*Calculation of the Rate of Electron Transfer*

This type of analysis provides a qualitative prediction of what type of PET process is possible and can provide some insight into the PET process, this can be quantified through calculation of the rate of electron transfer using Marcus theory.[37,38] This approach has been used to predict the rate of electron transfer in a range of systems, for examples see references.[39–41] According to Marcus theory the rate of electron transfer can be expressed as

$$k_{\mathrm{ET}} = \frac{2\pi}{\hbar}|V_{\mathrm{F-CT}}|^2 \frac{1}{\sqrt{4\pi\lambda k_B T}} \exp\left[\frac{-(\lambda+\Delta G)^2}{4\lambda k_B T}\right] \tag{4}$$

where $\lambda$ is the reorganisation energy, $\Delta$G is the total change in energy between the two states and $V_{\mathrm{F-CT}}$ is the electron transfer coupling which can be expressed as

$$V_{\mathrm{F-CT}} = \frac{\Delta E|\vec{\mu}_{\mathrm{F-CT}}|}{\sqrt{\Delta\mu^2_{\mathrm{F-CT}} + 4|\vec{\mu}_{\mathrm{F-CT}}|^2}} \tag{5}$$

in the generalised Mulliken-Hush scheme[42] within the two-state approximation. $\vec{\mu}_{\mathrm{F-CT}}$ is the transition dipole moment between the local excited fluorophore state and the CT state and $\Delta\mu_{\mathrm{F-CT}}$ is the difference between the permanent moments of the excited states. The $\Delta$SCF(sol) calculations give values of $\lambda$=0.75 eV and $\Delta$G=0.20 eV. The electron transfer coupling is computed in a gas phase TDDFT calculation at the ground state structure with the CAM-B3LYP calculation but rescaled according to the energy difference between the states in the condensed phase to give a value of 5.9 x $10^{-3}$ eV. Combined together these give a value of $k_{ET}$=5.98 x $10^6$ $s^{-1}$ for the rate of electron transfer, suggesting that the process occurs on the microsecond timescale.

# Conclusions

In this paper the electronic structure and associated fluorescence properties of a $K^+$ ion sensor have been modelled with DFT and TDDFT. Absorption and emission energies of the intense electronic excitation localised on the fluorophore are accurately described using a ΔSCF approach, which gives excitation energies closer to experiment than TDDFT. The PET processes that underpin the functioning of the sensor cannot be rationalised based upon analysis of the molecular orbital diagram arising from DFT calculations for the isolated molecule or with implicit solvent. To correctly account for the functioning of the sensor requires consideration of relative energies of the electronic states formed from the local excitation on the fluorophore and the lowest fluorophore→chelator CT state. The inclusion of solvent in these calculations is critical since the strong interaction of the CT state with the solvent lowers it energy below the local fluorophore excited state making a reductive PET possible in the absence of $K^+$, while no such process is possible when the sensor is bound to $K^+$. The rate of electron transfer can be quantified using Marcus theory, and the rate of electron transfer is computed to be $k_{ET}$=5.98 x $10^6$ $s^{-1}$.

# Acknowledgments

The authors are grateful to the University of Nottingham for a studentship for EAB and access to its High Performance Computing facility.

## References

(1) Kofuji, P.; Newman, E. A Potassium Buffering in the Central Nervous System. *Neuroscience* **2004**, *129*, 1045-1056.

(2) Stanton, B. A.; Biemesderfer, D.; Wade, J. B.; Giebisch, G. Structural and Functional Study of the Rat Distal Nephron: Effects of Potassium Adaptation and Depletion. *Kidney International* **1981**, *19*, 36-48.

(3) Gadsby, D. C.; Niedergerke, R.; Page, S. Do Intracellular Concentrations of Potassium or Sodium Regulate the Strength of the Heart Beat? *Nature* **1971**, *232*, 651-652.

(4) Mitchell, J. E.; Pyle, R. L.; Eckert, E. D.; Hatsukami, D.; Lentz, R. Electrolyte and Other Physiological Abnormalities in Patients with Bulimia. *Psychological Medicine* **1983**, *13*, 272-278.

(5) MacGregor, L. C.; Matschinsky, F. M. Altered Retinal Metabolism in Diabetes. *J. Bio. Chem.* **1986**, *261*, 4052-4058.

(6) Boens, N.; Leen, V.; Dehaen, W. Fluorescent Indicators Based on BODIPY. *Chem. Soc. Rev.* **2012**, *41*, 1130-1172.

(7) de Silva, A. P.; Gunaratne, H. Q. N.; Gunnlaugsson, T.; Huxley, A. J. M.; McCoy, C. P.; Rademacher, J. T.; Rice, T. E. Signaling Recognition Events with Fluorescent Sensors and Switches. *Chem. Rev.* **1997**, *97*, 1515-1566.

(8) Fan, L.-J.; Zhang, Y.; Murphy, C. B.; Angell, S. E.; Parker, M. F. L.; Flynn, B. R.; Jones Jr., W. E. Fluorescent Conjugated Polymer Molecular Wire Chemosensors for Transition Metal Ion Recognition and Signaling. *Coord. Chem. Rev.* **2009**, *253*, 410-422.

(9) Basarić N.; Baruah, M.; Qin, W.; Metten, B.; Smet, M.; Dehaen, W.; Boens, N. Synthesis and Spectroscopic Characterisation of BODIPY Based Fluorescent off-on Indicators with Low Affinity for Calcium. *Org. Biomol. Chem.* **2005**, *3*, 2755-2761.

(10) Keawwangchai, T.; Morakot, N.; Wanno, B. Fluorescent Sensors Based on BODIPY Derivatives for Aluminium Ion Recognition: An Experimental and Theoretical Study. *J. Mol. Model* **2013**, *19*, 1435-1444.

(11) Chibani, S.; Le Guennic, B.; Charaf-Eddin, A.; Maury, O.; Andraud, C.; Jacquemin, D. On the Computation of Adiabatic Energies in Aza-Boron- Dipyrromethene Dyes. *J. Chem. Theory Comput.*, **2012**, *8*, 3303-3313.

(12) Le Guennic, B.; Maury, O.; Jacquemin, D. Aza-boron-dipyrromethene Dyes: TD-DFT Benchmarks, Spectral Analysis and Design of Original Near-IR Structures. *Phys. Chem. Chem. Phys.*, **2012**, *14*, 157-164.

(13) Buyuktemiz, M.; Duman, S.; Dede, Y. Luminescence of BODIPY and Dipyrrin: An MCSCF Comparison of Excited States. *J. Phys. Chem. A*, **2013**, *117*, 1665-1669.

(14) Briggs, E. A.; Besley, N. A.; Robinson, D. QM/MM Excited State Molecular Dynamics and Fluorescence Spectroscopy of BODIPY. *J. Phys. Chem. A*, **2013**, *117*, 2644-2650.

(15) Jacquemin, D.; Chibani, S.; Le Guennic, B.; Mennucci, B. Solvent Effects on Cyanine Derivatives: A PCM Investigation. *J. Phys. Chem. A* **2014**, *118*, 5343-5348.

(16) Mukherjee, S.; Thilagar, P. Effect of Alkyl Substituents in BODIPYs: A Comparative DFT Computational Investigation. *RSC Adv.* **2015**, *5*, 2706-2714.

(17) Zhou, X.; Su, F.; Gao, W.; Tian, Y.; Youngbull, C.; Johnson, R.H.; Meldrum, D.R. Triazacryptand-Based Fluorescent Sensors for Extracellular and Intracellular $K^+$ Sensing. *Biomaterials* **2011**, *32*, 8574-8583.

(18) Werner, H.-J.; Knowles, P. J. An Efficient Internally Contracted MulticonfigurationÐReference Configuration Interaction Method. *J. Chem. Phys.* **1988**, *89*, 5803-5814.

(19) Celanai, P.; Werner, H.-J.; Multireference Perturbation Theory for Large Restricted and Selected Active Space Reference Wave Functions. *J. Chem. Phys.* **2000**, *112*, 5546-5557.

(20) Salman, H.; Tal, S.; Chuvilov, Y.; Solovey, O.; Abraham, Y.; Kapon, M.; Suwinska, K.; Eichen, Y. Sensitive and Selective PET-Based Diimidazole Luminophore for $Zn^{II}$ Ions: A Structure-Activity Correlation. *Inorg. Chem.* **2006**, *45*, 5315-5320.

(21) Bañuelos, J.; López Arbeloa, F.; Arbeloa, T.; Salleres, S.; Amat-Guerri, F.; Liras, M.; López Arbeloa, I. Photophysical Study of New Versatile Multichromophoric Diads and Triads with BODIPY and Polyphenylene Groups. *J. Phys. Chem. A* **2008**, *112*, 10816-10822.

(22) Lu, H.; Zhang, S.; Liu, H.; Wang, H.; Shen, Y.; Liu, C.; You, X. Experimentation and Theoretic Calculation of a BODIPY Sensor Based on Photoinduced Electron Transfer for Ions Detection. *J. Phys. Chem. A* **2009**, *113*, 14081-14086.

(23) Lee, H.; Hancock, R. D.; Lee, H.-S. Role of Fluorophore-Metal Interaction in Photoinduced Electron Transfer (PET) Sensors: Time-Dependent Density Functional Theory (TDDFT) Study. *J. Phys. Chem. A* **2013**, *117*, 13345-13355.

(24) Peach, M.J.G.; Benfield, P.; Helgaker, T.; Tozer, D.J. Excitation Energies in Density Functional Theory: An Evaluation and a Diagnostic Test. *J. Chem. Phys.* **2008**, *128*, 044118 1-8.

(25) Hamprecht, F. A.; Cohen, A. J.; Tozer, D. J.; Handy, N. C. Development and Assessment of New Exchange-Correlation Functionals. *J. Chem. Phys.* **1988**, *109*, 6264-6271.

(26) Hehre, W. J.; Ditchfield, R.; Pople, J. A. Self-Consistent Molecular Orbital Methods. XII. Further Extensions of Gaussian-Type Basis Sets for use in Molecular Orbital Studies of Organic Molecules. *J. Chem. Phys.* **1972**, *56*, 2257-2261.

(27) Rassolov, V.; Pople, J. A.; Ratner, M.; Windus, T. L. 6-31G* Basis Set for Atoms K Through Zn. *J. Chem. Phys.* **1998**, *109*, 1223-1229.

(28) Yanai, T.; Tew, D.P.; Handy, N.C. A New Hybrid Exchange-Correlation Functional Using the Coulomb-Attenuating Method (CAM-B3LYP). *Chem. Phys. Lett.* **2004**, 393, 51-57.

(29) Gilbert, A. T. G.; Besley, N. A.; Gill, P. M. W. Self-Consistent Field Calculations of Excited States Using the Maximum Overlap Method, (MOM). *J. Phys. Chem. A* **2008**, *112*, 13164-13171.

(30) Robinson, D; Besley, N. A. Modelling the Spectroscopy and Dynamics of Plastocyanin. *Phys. Chem. Chem. Phys.* **2010**, *12*, 9667-9676.

(31) Ershova, O. V.; Besley, N. A. Theoretical Calculations of the Excited State Potential Energy Surfaces of Nitric Oxide. *Chem. Phys. Lett.* **2011**, *513*, 179-183.

(32) Ershova. O. V.; Besley, N. A. Can Density Functional Theory Describe the NO($X^2\Pi$)-Ar and NO($A^2\Sigma^+$)-Ar Van der Waals Complexes? *J. Chem. Phys.*, **2012**, *136*, 244313 1-9.

(33) Ziegler, T.; Rauk, A.; Baerends, E.J. Calculation of Mulitplet Energies by Hartree-Fock-Slater Method. *Theor. Chim. Acta*, **1977**, *43*, 261-271.

(34) Hanson-Heine, M. W. D.; George, M. W.; Besley, N. A. Calculating Excited State Properties Using Kohn-Sham Density Functional Theory. *J. Chem. Phys.*, **2013**, *138*, 064101 1-8.

(35) Shao, Y.; Gan, Z.; Epifanovsky, E.; Gilbert, A.T.B.; Wormit, M.; Kussmann, J.; Lange, A.W.; Behn, A.; Deng, J.; Feng, X.; et al. Advances in Molecular Quantum Chemistry Contained in the Q-Chem 4 Program Package. *Mol. Phys.*, **2015**, *113*, 184-215.

(36) Robinson, D.; Besley, N.A.; Lunt, E.A.M.; O'Shea, P.; Hirst, J.D. Electronic Structure of 5-hydroxyindole: From Gas Phase to Explicit Solvation. *J. Phys. Chem. B* **2009**, *113*, 2535-2541.

(37) Marcus, R. A. On the Theory of Oxidation-Reduction Reactions Involving Electron Transfer. V. Comparison and Properties of Electrochemical and Chemical Rate Constants. *J. Phys. Chem.*, **1963**, *67*, 853-857.

(38) Marcus, R. A.; Sutin, N. Electron Transfers in Chemistry and Biology. *BioChem. Biophys. Acta*, **1985**, *811*, 265-322.

(39) Hsu, C.-P. The Electronic Couplings in Electron Transfer and Excitation Energy Transfer. *Acc. Chem. Res.*, **2009**, *42*, 509-518.

(40) Subotnik, J.E.; Vura-Weis, J.; Sodt, A.J.; Ratner, M.A. Predicting Accurate Electronic Excitation Transfer Rates via Marcus Theory with Boys or Edmiston-Ruedenberg Localized Diabatization. *J. Phys. Chem. A*, **2010**, *114*, 8665-8675.

(41) Manna, A.K.; Dunietz, B.D. Communication: Charge-Transfer Rate Constants in Zinc-Porphyrin-Porphyrin-Derived Dyads: A Fermi Golden Rule First-Principles-Based Study. *J. Chem. Phys.*, **2014**, *141*, 121102 1-5.

(42) Cave, R. J.; Newtin, M. D. Generalization of the Mulliken-Hush Treatment for the Calculation of Electron Transfer Matrix Elements. *Chem. Phys. Lett.*, **1996**, *249*, 15-19.

| Method | $\Delta E^{F\rightarrow F}_{noK^+}$ / eV | $\Delta E^{F\rightarrow F}_{K^+}$ / eV |
|---|---|---|
| $\Delta\varepsilon$ | 3.76 | 3.83 |
| TD-B97-1 | 3.36 | 3.47 |
| TD-CAM-B3LYP | 3.76 | 3.86 |
| $\Delta$SCF$^{SM}$-B97-1 | 2.82 | 2.94 |
| $\Delta$SCF$^{SP}$-B97-1 | 3.20 | 3.36 |
| $\Delta$SCF$^{SM}$(sol)-B97-1 | 2.71 | 2.79 |
| $\Delta$SCF$^{SP}$(sol)-B97-1 | 3.02 | 3.12 |
| Exp. | 2.76 | - |

**Table 1**: Computed transition energies for the intense transition localised on the fluorophore with and without the $K^+$ ion for a range of computational methods.

| Method | 6-31G* | 6-311G* | 6-31+G* |
|---|---|---|---|
| $\Delta\varepsilon$ | 3.76 | 3.76 | 3.70 |
| TD-B97-1 | 3.36 | 3.33 | 3.42 |
| TD-CAM-B3LYP | 3.76 | 3.71 | 3.84 |
| $\Delta SCF^{SM}$-B97-1 | 2.82 | 2.86 | 2.80 |
| $\Delta SCF^{SP}$-B97-1 | 3.20 | 3.23 | 3.17 |

**Table 2**: Variation in the computed transition energies for the intense transition localised on the fluorophore without $K^+$ ion bound ($\Delta E^{F\rightarrow F}_{noK^+}$) in eV.

| Method | $\Delta E^{F\rightarrow C}_{noK^+}$ / eV | $\Delta E^{F\rightarrow C}_{K^+}$ / eV |
|---|---|---|
| TD-B97-1 | 2.78 | 3.65 |
| TD-CAM-B3LYP | 4.36 | 4.34 |
| $\Delta SCF^{SM}$-B97-1 | 5.05 | 3.74 |
| $\Delta SCF^{SM}$(sol)-B97-1 | 2.57 | 3.29 |

**Table 3**: Computed transition energies for the lowest energy fluorophore→chelator charge transfer transition with and without the $K^+$ ion for a range of computational methods

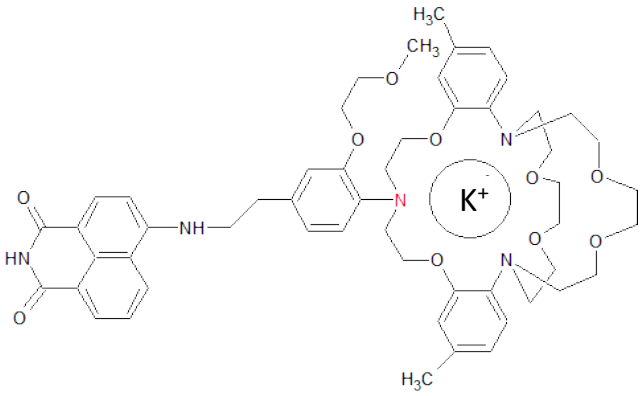


**1**

Figure 1: Model of the $K^+$ fluorescent sensor.

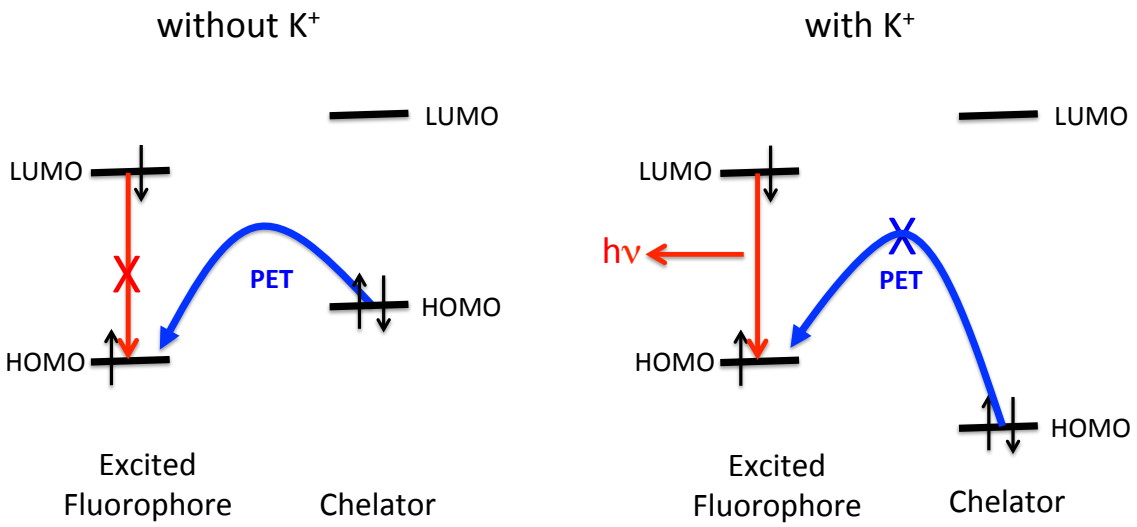


Figure 2: Schematic representation of the photoinduced electron transfer process in the $K^+$ sensor.

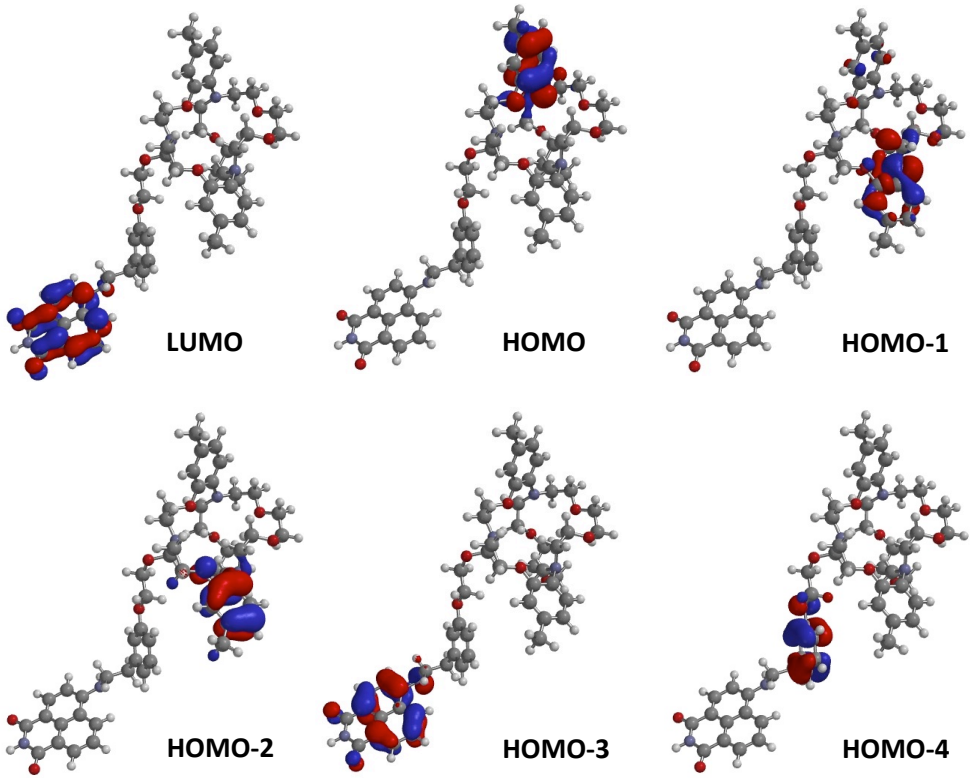


Figure 3: Molecular orbitals of the $K^+$ sensor without $K^+$.

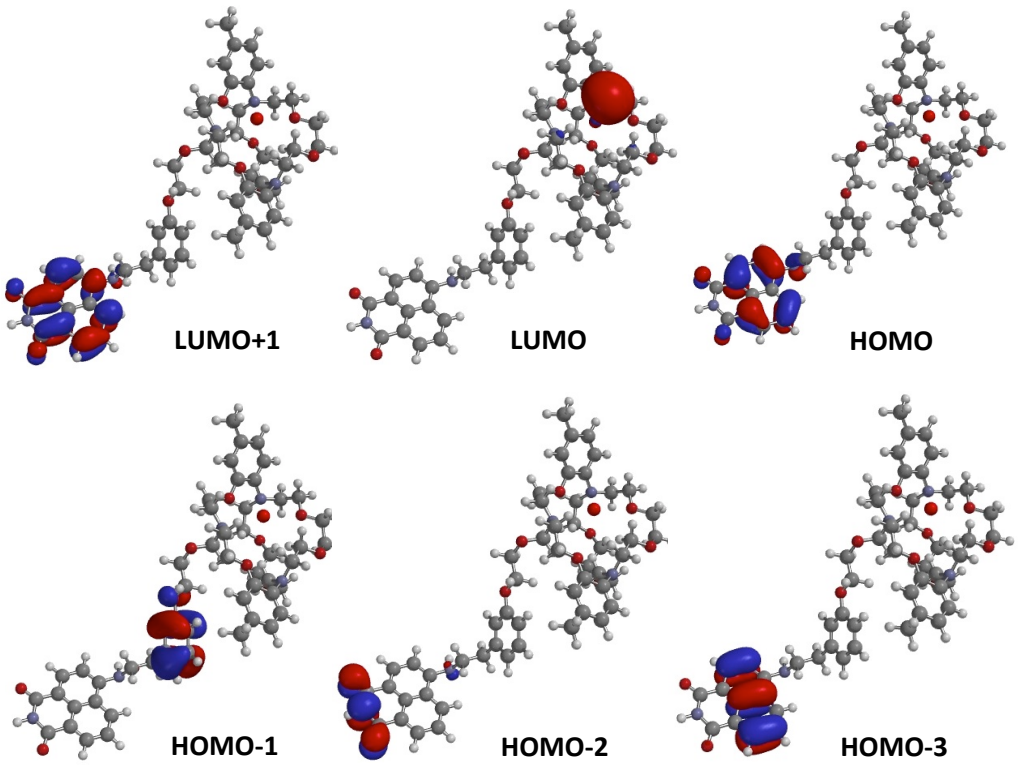


Figure 4: Molecular orbitals of the $K^+$ sensor with $K^+$.

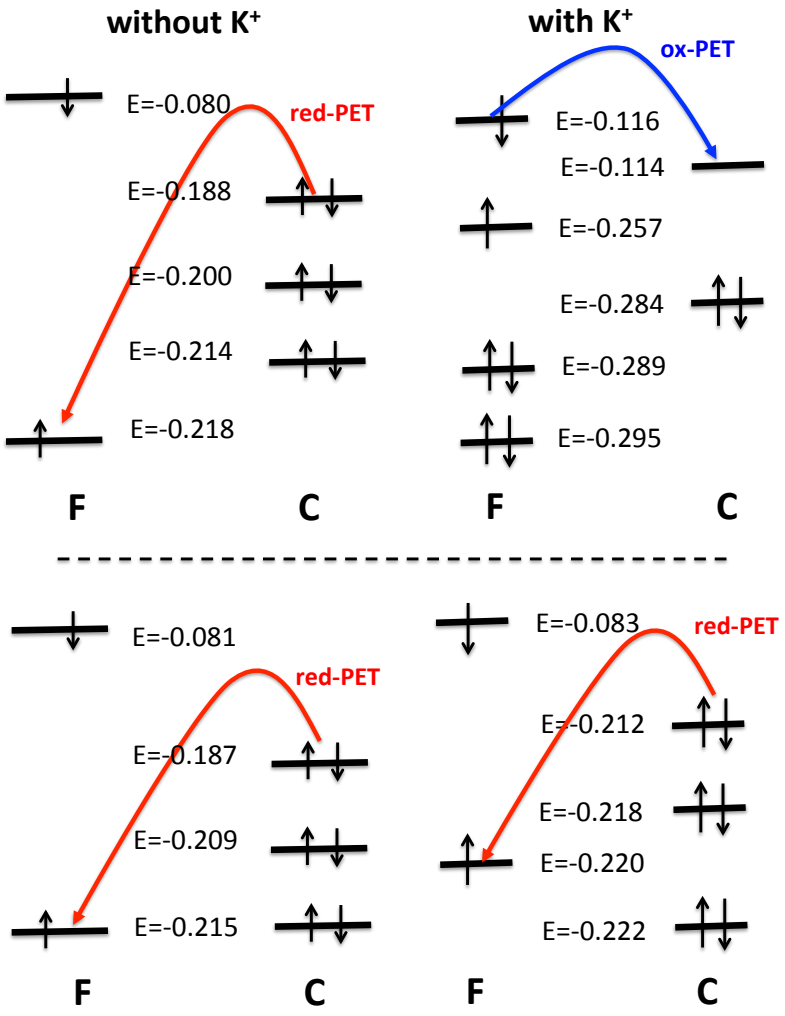


Figure 5: Molecular orbital diagram based upon the ground state B97-1/6-31G* calculation for the gas phase (upper panel) and in solution (lower panel). F represents orbitals localised on the fluorophore and C represents orbitals localised on the cheating part of there molecule, orbital energies in a.u.

For Table of Contents

A Density Functional Theory Based Analysis of Photoinduced Electron Transfer in a Triaza-cryptand Based $K^+$ Sensor

by Edward A. Briggs and Nicholas A. Besley